



Swansea University
Prifysgol Abertawe



Cronfa - Swansea University Open Access Repository

This is an author produced version of a paper published in:

Journal of The Electrochemical Society

Cronfa URL for this paper:

<http://cronfa.swan.ac.uk/Record/cronfa37405>

Paper:

Rajamani, A., Jothi, S., Datta, M. & Rangarajan, M. (2018). Electrodeposition of Tin-Bismuth Alloys: Additives, Morphologies and Compositions. *Journal of The Electrochemical Society*, 165(2), D50-D57.

<http://dx.doi.org/10.1149/2.1281714jes>

This item is brought to you by Swansea University. Any person downloading material is agreeing to abide by the terms of the repository licence. Copies of full text items may be used or reproduced in any format or medium, without prior permission for personal research or study, educational or non-commercial purposes only. The copyright for any work remains with the original author unless otherwise specified. The full-text must not be sold in any format or medium without the formal permission of the copyright holder.

Permission for multiple reproductions should be obtained from the original author.

Authors are personally responsible for adhering to copyright and publisher restrictions when uploading content to the repository.

<http://www.swansea.ac.uk/library/researchsupport/ris-support/>

Electrodeposition of Tin-Bismuth Alloys: Additives, Morphologies and Compositions

A. R. Rajamani, Sathiskumar Jothi, Madhav Datta, Murali Rangarajan

Abstract

Electrodeposition of tin-bismuth alloys on polycrystalline copper electrodes has been studied from an acidic bath comprising SnCl_4 , $\text{Bi}(\text{NO}_3)_3$, citric acid, poly(vinyl alcohol) and betaine. Using linear sweep voltammetry (LSV) and chronoamperometry (CA), co-deposition of tin and bismuth from the above bath has been examined. Bismuth (III) ions get reduced in a single-step, three-electron-transfer reaction while tin (IV) ions undergo a two-step reduction through the formation of tin (II) ions. Nitric acid in the bath not only enhances solubility of the precursors but also decreases the peak potential separation between bismuth (III) and tin (II) ions. Through the introduction of various additives and variation in bath pH, co-deposition is preserved while the composition of tin in the obtained alloy is modified. The morphologies, composition and crystallinity of the deposits have been determined using scanning electron microscopy, inductively coupled plasma atomic emission spectroscopy and X-ray diffraction, respectively. A wide range of alloy compositions (from 14% to 75% tin), including the eutectic Sn-Bi alloy have been deposited. Novel morphologies such as yarns-of-spool have been obtained.

Keywords: Electrodeposition, Tin-Bismuth Alloy, Eutectic, Additives

1 Introduction

Eutectic Pb-Sn alloys are still the most widely used interconnect materials for integrated circuit packaging. These alloys exhibit minimum electrical contact resistance, reliability, excellent solderability, good hardness and corrosion resistance [1-2]. However, since the use of Pb-Sn alloys has been restricted due to the toxicity of lead in these alloys, which has led to the development of many lead-free alloys. As replacement for lead, materials like silver, tin, copper, zinc, antimony, bismuth and indium have been studied [3-7]. Among the candidate lead-free alloys, eutectic tin-bismuth alloys have specific advantages including low melting point, low Young's modulus and low thermal conductivity, as indicated in Table 1 [8-9]. The lower melting point facilitates lower joining temperatures, the low Young's modulus allows for compliance in absorbing stress, and low thermal conductivity implies less transfer of thermal stress to the low-k

dielectrics in the circuits. Further, the use of a eutectic alloy minimizes electrical contact defects arising from unwanted vibrations before the complete solidification of the interconnect.

Tin-bismuth alloys have been electrodeposited from different baths using direct-current and pulsed-current techniques [10-25]. The standard reduction potential of Bi^{3+} is 444 mV nobler than that of Sn^{2+} . Thus, the challenge of depositing Sn-Bi alloys of varying Bi composition is considerable. Effects of complexing agents to reduce the deposition potential difference have been studied. The addition of surfactants to suppress the deposition of one of the species has also received consideration. Fukuda *et al.* have studied the effects of polyoxyethylene lauryl ether or POELE on the deposition of Sn-Bi alloys from a SnSO_4 , H_2SO_4 and $\text{Bi}(\text{NO}_3)_3$ bath with 10:1 ratio of Sn^{2+} to Bi^{3+} , and small concentrations of POELE [16]. It is found that POELE suppresses Bi deposition, enabling formation of low concentration Bi alloys, 97Sn3Bi, for example. Further, it also smoothens the deposit surface and reduces dendritic growth by adsorbing on both Sn and Bi deposit and inhibiting further deposition. Medvedev *et al.* also examined formation of low concentration Bi alloys (0.1 to 1.3%) using sulfate baths (SnSO_4 , $\text{Bi}_2(\text{SO}_4)_3$, H_2SO_4) with Sn^{2+} to Bi^{3+} concentration ratios ranging from 5:1 to 25:1, in the presence of organic additives such as sintanol, formalin and benzyl alcohol [17]. The current efficiency of deposition increases with increasing Sn^{2+} to Bi^{3+} ratio. High leveling power and bright deposits are obtained for current densities of 4-6 A/dm^2 . However, there are significant challenges in dissolving the bath constituents in preparing the electrolyte.

A 30Sn70Bi electrodeposit has been obtained by Tsai *et al.* using a SnCl_4 and $\text{Bi}(\text{NO}_3)_3$ bath (0.1M each), with citric acid, EDTA and PEG as additives on Ni-coated copper cathodes with graphite anodes [11]. It is found that citric acid and EDTA significantly reduce the potential gap between the deposition of Bi and Sn. PEG has also been studied in the same work as possible surfactant. It primarily suppresses Bi deposition and hydrogen evolution. EDTA may also facilitate reduction of Sn^{4+} on the surface, similar to the well-known behavior of tartarates [18]. Based on a fractional factorial design study, Tsai and Hu found that pH, plating current density and citric acid concentration are the key factors influencing the composition of Sn-Bi deposits [19, 20]. Highest Sn content (64%) has been obtained at pH of 6.5, 20 mA/cm^2 current density and 0.3 M citric acid concentration. The tin content on the deposit varies linearly with the ratio of Sn^{4+} to $[\text{Sn}^{4+} + \text{Bi}^{3+}]$, thereby providing a means to control and predict the deposit composition. All deposits show uniform polyhedral crystallites, with rough and porous surfaces,

despite the addition of PEG. The growth and orientation of Sn and Bi crystallites are composition-dependent.

Near eutectic 60.75Sn-Bi alloy was electroplated by Goh *et al.* from methane sulfonic bath in the presence of hydroquinone and gelatin at 18 mA/cm² [21] and the effects of reflow temperature, interfacial intermetallic compound morphology, shear strength and fracture mechanism of the Sn-Bi/Cu solder joints have been investigated [22]. Methane sulfonate baths have been explored [23-25] for deposition of the eutectic 42Sn58Bi composition. The organic sulfonate bath eliminates the precipitation of Bi-salts in sulfate baths above 10% Bi concentration. Talin HSM 96 has been used as grain refiner in this work. Electroplating is carried out using both DC and pulsed current. The additive has the effects of raising the overpotential for electrodeposition through adsorption on the surface, refining the surface structure by eliminating dendritic structures, and reducing the potential gap between the deposition of Sn and Bi. It is found that when Sn-Bi alloy was electrodeposited through pulsed current with a peak current density of 4 A/dm², Sn content in the deposit increases with increasing pulse frequency and decreasing duty cycle. In addition, the Sn-Bi deposits become finer with decreasing pulse frequency and increasing duty cycle.

Joseph *et al.* have studied the effect of surfactant on the bath stability and near eutectic electrodeposition of Sn-Ag-Cu films from a methane sulfonic acid bath with increase in current density beyond 5 mA/cm². The deposited films have compact microstructure with grain size in the range 6-8 μm and thickness in the range 20-100 μm. The co-deposition of Sn-Bi-Cu films using a stable stannic salt bath has also been studied. There is improvement in the microstructure with Bi rich state, with close to 90 wt. % Bi for deposition at 5 mA/cm² [26-28].

In such works, the challenge is to design process variables to demonstrate control over the composition of the alloys (including the eutectic), as well as the deposition of reasonably smooth morphologies. The mechanism of co-deposition of tin and bismuth from the chosen bath needs to be understood clearly so as to develop strategies of controlling composition of the deposited alloys. This work reports a cyanide-free, sulfonic-acid-free electrodeposition of tin-bismuth alloys onto polycrystalline copper cathodes with stainless steel anodes, from an acidic bath containing tin (IV) chloride, bismuth (III) nitrate, nitric acid, and the additives citric acid, poly(vinyl alcohol) and betaine. Use of insoluble anodes such as stainless steel has an important

advantage of eliminating fluctuations in current distributions due to changing dimensions as in the case of soluble anodes. This is particularly important when such alloys should be electrodeposited onto patterned templates, as in the case of fabrication of solder bumps for flip-chip joining. In this study, using linear sweep voltammetry and chronoamperometry, co-deposition of tin and bismuth from the above bath has been studied. Galvanostatic deposition of tin and bismuth reveals that a wide range, viz., 14% to 75% of tin composition in the deposit may be achieved under different deposition conditions. The morphologies and crystallinities of the deposits have been examined using scanning electron microscopy and X-ray diffraction.

2 Materials and Methods

All chemicals used were of analytical grade, and ultrapure water (Millipore, 18 M Ω) was used throughout. In the voltammetric and amperometric studies, a three-electrode system comprising polycrystalline copper working electrode (0.2 \times 0.2 cm²), platinum wire counter electrode, and Ag/AgCl reference electrode was used. Galvanostatic deposition was carried out with a two-electrode system of a polycrystalline copper cathode (2 \times 2 cm²) and stainless steel anodes on either side of the cathode. All electrochemical experiments were carried out using a WaveNow potentiostat (Pine Instruments, Inc.). Before the studies, the copper electrode was immersed in acetic acid for five minutes. Then it was subjected to ultrasonication in acetone for two minutes and ultrapure water for an additional two minutes. This was done to remove the air formed oxide layers present. All studies were carried out at ambient conditions. The deposited electrode was rinsed with ultrapure water for a few times, dried under ambient conditions and stored in a desiccator. High-resolution scanning electron microscopy (HRSEM) imaging was carried out with a FEI Quanta FEG 200 scanning electron microscope. Alloy composition was measured on an inductively coupled plasma atomic emission spectrometer (ICP-AES), SPECTRO ARCOS. X-ray diffraction (XRD) studies were conducted on a Rigaku (Miniflux-600) X-ray diffractometer.

3 Results and Discussion

3.1 Linear Sweep Voltammetry

The reduction of tin (IV) and bismuth (III) from an acidic bath with and without different additives (Table 2) was investigated using linear sweep voltammetry. It is seen that bismuth (III) reduction is a single-step, three-electron-transfer process with a peak potential of -82 mV (Fig. 1a), [29-31] whereas tin (IV) reduction is a two-step process, with a sharp peak at -202 mV and an increasing current starting from -502 mV (Fig. 1b), with the latter corresponding to Sn^{4+} reduction to Sn^{2+} , and the former to the reduction of Sn^{2+} ions. Thus, in the acidic nitrate bath used in this study, the separation of peak potentials of deposition of bismuth (III) and tin (II) is about 120 mV. However, in a bath containing both Sn^{4+} and Bi^{3+} ions (Fig. 2a), there are only two peaks (-282 mV and -612 mV), the former being a composite peak for Sn^{2+} and Bi^{3+} reduction, and the second peak corresponding to Sn^{4+} reduction. Thus, co-deposition of bismuth and tin is enabled in the bath. Nitric acid in the bath helps not only in the dissolution of tin (IV) chloride and bismuth (III) nitrate, but also the co-deposition of the two metals.

That tin reduction is a two-step process is further established in the presence of additives, viz., citric acid, poly(vinyl alcohol), and betaine (Fig. 2b), where there are three reduction peaks corresponding to Bi^{3+} (-178 mV), Sn^{2+} (-243 mV), and Sn^{4+} (-508 mV) reduction. These results indicate that tin (II) and bismuth (III) can be co-deposited from this bath within a narrow 65 mV potential window. The peak potentials corresponding to their reduction are both shifted cathodically. Bismuth (III) reduction potential has shifted by -96 mV, thereby enabling co-deposition. Increasing the pH of the bath to 3.0 (Fig. 2c) and 6.0 (Fig. 2d) preserves the ability for co-deposition, while further narrowing the potential difference between Sn^{2+} and Bi^{3+} reduction.

It is instructive to compare the peak current densities corresponding to the reduction of tin (IV), tin (II) and bismuth (III) shown in Fig. 1 and Fig. 2. These are presented in Table 3. The peak current densities obtained from the voltammetric experiments shed light on the possible compositions of the deposited alloys, and on possible strategies to control the composition of electrodeposited tin-bismuth alloys from this bath. Compared to the individual – tin only and bismuth only – bath, the peak current densities of the reduction of the ions from the bath containing both ions are significantly higher, through higher cathodic overpotentials are

necessary for reduction, possibly for simultaneous nucleation of the bismuth-rich and tin-rich phases.

The rate of tin (IV) reduction in the presence of bismuth (III) ions is suppressed by the introduction of bath additives (by about 53 %), and increased pH (76 % reduced current at pH 3.0 and 80 % reduced current at pH 6.0). This is also seen in the level-off limiting current densities for tin (IV) reduction. In the presence of bath additives, at pH 0.4, the peak current densities of bismuth (III) and tin (II) are nearly equal. This matches closely with the composition observed from the ICP-AES analysis, reported in Table 4. The peak potentials for tin (IV) reduction are also shifted further cathodically with increase in bath pH. Such clear trends are not discernible for tin (II) and bismuth (III) reductions, particularly because their reduction potentials in the bath are too close to each other. However, a slower reduction of tin (IV) ions have to naturally imply smaller bath concentrations of tin (II) ions. Thus, it is expected that the bismuth concentration should increase in the deposited films with the introduction of additives and increase of bath pH. This is indeed evidenced from the ICPAES results reported in Table 4.

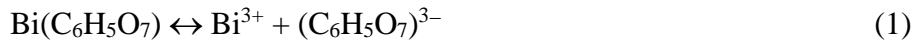
Figs. 3 through 5 demonstrate the effects of concentrations of the three additives on the deposition process. It is clear from Fig. 3, that there is only a mild change in the peak currents corresponding to the composite peak for the co-reduction of Bi^{3+} and Sn^{2+} ions due to the introduction of citric acid in the bath. However, increasing citric acid concentration suppresses the rate of reduction of which Sn^{4+} ions by about 30%. This effect is not very pronounced beyond a citric acid concentration of 0.2 M. Therefore, the concentration of citric acid in the plating bath was fixed to be 0.2 M.

The presence of the chloride and nitrate anions, along with citric acid, can result in the tin and bismuth ions being present in different complex forms. Buckle [32] has determined the Pourbaix diagrams for such systems, which give clues to the states of these ions. Both tin (II) and tin (IV) ions predominantly exist as chloride complexes, $[\text{SnCl}_4]^{2-}$ and $[\text{SnCl}_6]^{2-}$ respectively, in aqueous solutions with high chloride concentrations. This results in a cathodic shift of the equilibrium potential of tin (IV) reduction [32]. However, tin (II) ions may also be present as SnCl^+ , while tin (IV) ions may also be present as $[\text{SnCl}_3]^-$ at high chloride concentrations and as HSnO_2^- , SnO_3^{2-}

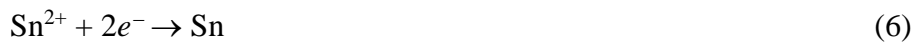
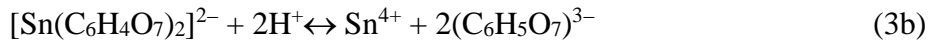
at high pH. Both chloride ions and nitrate ions result in the formation of SnNO_3^+ or SnCl^+ from HSnO_2^- and SnO_3^{2-} ions, either through chemical or electrochemical routes. Further, Sn^{2+} may also be formed from solution reduction of Sn^{4+} [32].

It is also known that citric acid forms complexes with tin (IV) through the anodic dissolution of SnO_2 [33], with tin (II) [34] and bismuth (III) [35] ions. Tin (IV)-citrate complex is hexacoordinated (octahedral) while in the tin (II)-citrate complex, three of the six protons associated with the six carboxylic groups and two protons associated with the hydroxyl groups are dissociated. Based on the complexes, it may be deduced that the cathodic reduction of bismuth (III) in a citric acid-containing bath is likely to be a CE reaction (reaction 1 followed by 2, as shown below) while that of tin (IV) is a more complex CEE (reactions 3a or 3b, followed by 4 and 6 as shown below) or CECE (reactions 3a/3b, 4, 5a/5b, 6) reaction. (Here, C stands for a chemical reaction while E stands for an electron transfer reaction.) The exact structures of the citrate complexes are dependent on the ions in the bath and pH, and they need to be established. The relative rates of release of the respective ions from their citrate complexes have also not been established in the literature to the best of our knowledge. It is also not clear as to whether the ion release or its reduction is the slowest step. From this study, it may be stated that, ultimately, bismuth reduction is generally faster in this bath than that of tin.

Bi^{3+} Reduction in Citric Acid-Containing Baths:



Sn^{4+} Reduction in Citric Acid-Containing Baths:



The effect of PVA on the reduction of bismuth (III) and tin (II) and (IV) ions is shown in Fig 4. Poly(vinyl alcohol) is known to adsorb onto copper substrate [36-38], suppressing the number density of active sites for nucleation. Thus, the peak current densities are reduced significantly, particularly for bismuth (III) ions. In fact, one of the clearest features evident in Fig. 4 is the separation of reduction potentials of bismuth (III) (-180 mV) and tin (II) (-270 mV) ions, with bismuth (III) peak current density being lower than that of tin (II) and even tin (IV). Comparison of Fig. 4 with Fig. 2b reveals that in the presence of both citric acid and poly(vinyl alcohol), this peak separation between bismuth (III) and tin (II) reduction is maintained (i.e., at -282 mV (co-deposit) in the absence of PVA vs. peak separation -65 mV in the presence of PVA). Also, the peak current of bismuth (III) reduction (at -280 mV) is higher with citric acid (-0.149 mA/cm²) than without citric acid (-0.132 mA/cm²). Thus, while PVA appears to preferentially suppress bismuth (III) reduction, citric acid suppresses tin (IV) and tin (II) reduction more strongly. Such combinations of additives are typically preferred for their ability to effectively modulate the alloy compositions. Further, it is observed that the effect of PVA is similar for concentrations above 5 gpl. Therefore, a PVA concentration of 5 gpl was chosen for the plating bath.

Betaine is typically used as a leveler in a plating bath to refine grains and features so that smooth deposits are obtained [39]. Introducing betaine in the bath, as seen by Fig. 5, does not significantly alter the peak current density or the limiting current density of tin (IV) reduction. Similar to citric acid, there is only a composite peak for the co-reduction of bismuth (III) and tin (II) ions, whose peak current is an inverse function of betaine concentration. At concentrations of betaine above 0.1 M, significant suppression effects are observed. Thus, it was determined that a betaine concentration of 0.05 M was sufficient for the leveling effect desired in the plating bath.

3.2 Chronoamperometry

Chronoamperograms were obtained at different potentials, -0.1 V to -0.6 V (in steps of -0.1 V), and the results are shown in Fig. 6. At -0.1 and -0.2 V, the overpotential is not sufficient to cause sufficient deposition of tin and bismuth. Therefore, at short times, the current is nearly constant, indicative of very slow kinetics. At long enough times, the current gradually decays. However, even at overpotentials greater than the peak potentials for Sn²⁺ and Bi³⁺ reduction, the current decay does not show an exponential trend that is typical of diffusion-controlled reactions.

Bismuth reduction is a mass-transfer-limited, diffusion-controlled reaction, as established in previous work [30, 31]. Therefore, this result implies that tin reduction is significantly activation-controlled. This is to be expected based on the LSV results because Sn^{4+} reduction occurs at -612 mV, whereas the cathodic overpotential is not that large. At short times, the current decreases slowly, and the overall current-time relationship indicates a sigmoidal dependence. This implies slow deposition kinetics at short times and gradually increasing effect of mass transfer at longer times. Nucleation occurs progressively on both the copper substrate as well as the growing crystals, as evidenced by the scanning electron microscopy images. In fact, as the number of nuclei increases, the surface concentration of the metal ions would be expected to drop, lessening the significance of slow kinetics and making diffusion more important. This might explain the shape of the chronoamperogram. To further describe the nucleation-growth behavior of alloys, many studies [40-42] resort to the use of models such as Scharifker-Hills model, and compare the current time transients to the predictions for instantaneous or progressive nucleation. Such comparisons could be valid if the reduction kinetics of the two metals are almost similar, they form isomorphous alloy films, and no other side reactions (ex. hydrogen evolution) take place. However, such comparisons may not be appropriate when:

- The reduction kinetics of the metals are dissimilar,
- Two or more solid phases nucleate simultaneously (ex. tin-rich and bismuth-rich phases, as observed in typical eutectic alloy systems), and,
- Secondary reactions take place (ex. nitrate reduction, reduction of tin (IV) ions) [38, 43].

In the absence of mathematical models accounting for such cases, only a qualitative discussion is presented.

Figs. 6(b-d), shows the current-transients of bismuth deposition from the nitric acid bath when additives, viz., citric acid, PVA and betaine, have been added, at pH values of 0.4, 3.0 and 6.0, respectively. The reduction reactions are more complex in the presence of additives (Equations 1 to 6). Whereas sigmoidal-shaped transients indicative of slow kinetics are observed in the absence of additives, power law behavior is observed consistently when additives are introduced in the bath, especially at longer times. Unlike the deposition of a single metal, here the power law exponent indicates the composite effect of simultaneous co-reduction of three ions, viz., Bi

(III), tin (IV) and tin (II). Further, the nucleation phenomena involved in the formation of multiple solid phases in alloy deposition is highly complex. In the presence of the bath additives, the power law coefficients tend to be between -0.335 to -0.427 for potentials up to -0.4 V. This indicates that diffusion plays a major role in the reduction of bismuth (III) ions [38]. At -0.5 V and -0.6 V, the coefficients are -0.175 and -0.198 , respectively. This is more gradual than the Cottrell behavior, possibly indicating slower reduction of tin (IV) ions. Increasing the pH of the solution, however, possibly alters the nucleation phenomena significantly.

At a pH of 3.0 and 6.0, at -0.1 V, the current densities are much smaller whereas they are almost indistinguishably similar at larger potentials. The power-law exponents for potentials -0.2 V to -0.6 V are around -0.78 for solution pH of 3.0 while they are around -0.71 for pH of 6.0. These are much steeper than typical Cottrell behavior, possibly indicative of strong diffusion effects in nucleation and growth of the alloy crystallites.

Thus, to summarize, chronoamperograms show significant competition between diffusion of the metal ions (or their complexes) and the reduction reactions in determining the overall rate of deposition under different driving forces. In the absence of additives, the reduction kinetics is likely the rate-limiting process as shown by the sigmoidal transients. Introducing bath additives reduce the observed current densities and slow down co-deposition, making diffusion or the availability of the metal ions at the surface more significant in determining deposition rate. These effects are more pronounced at higher pH values.

3.3 Alloy Composition and Crystallinity

Electroplating of Sn-Bi alloys were carried out using a two-electrode system comprising polycrystalline copper cathode and stainless steel anodes (on either side of the cathode). Electrodeposition experiments were conducted at a constant current density of 5 mA/cm^2 . Fig. 7 (a & b) shows SEM images of the Sn-Bi alloy obtained from the bath in the absence of additives. Novel yarn-spool-like morphologies (rich in bismuth) and needle-like micron- and sub-micron-sized crystallites (rich in tin) have been observed. ICP-AES analyses reveal that tin-bismuth eutectic alloy (41.3 % Sn and 58.7 % Bi) may be obtained using insoluble anodes. Adding citric acid, polyvinyl alcohol, and betaine suppresses the deposition rates of tin and bismuth. The complexing nature of citric acid and surface inhibiting behavior of PVA suppress the formation

of large features such as the yarn-of spools. They also significantly improve deposit adhesion. However, they result in tin-rich deposits because tin (II) reduction is enhanced. Additives suppress formation of large crystallites and needle-like structures, and favor of the formation of significantly homogeneous thin films with good surface coverage (Fig. 7 (c & d)).

Increasing the bath pH significantly inhibits tin reduction. Bismuth composition in the bath increases from 45.6 wt % (at pH 0.4) to 63.5 % (at pH 3.0) and to 86.0 % (at pH 6.0). At pH 3.0, nodular and cracked morphologies are seen with bright bismuth regions partially covered by the darker tin regions (Fig. 7 (e & f)). At pH 6.0, the deposition is slowed down significantly so that only poor surface coverage is obtained, with small crystallites (Fig. 7 (g & h)). From voltammetric studies, it is seen that tin reduction is slower than bismuth reduction. Thus, it is understandable that with increasing pH, bismuth composition in the deposits increases. Typically, it is seen that the bismuth-rich crystallites are larger in size than the tin-rich crystallites. It is interesting that the alloy films obtained at pH 3.0 have a nodular morphology. It appears as if there are much more tin-rich nuclei (per unit area) than bismuth rich nuclei. However, due to slower tin reduction kinetics, the bismuth-rich nuclei grow faster, which could have resulted in the observed morphology.

Fig. 8 shows XRD patterns of Sn-Bi alloy electrodeposits, Sn(2 0 0) and Bi(0 1 2) are the preferred orientations of Sn and Bi, respectively. Sn content of electrodeposits varies from 14 % to 75 % as obtained from ICP-AES measurements (Tables 4). Further, in Fig. 8a intensities of Sn(2 0 0) and Bi(0 1 2) are nearly equal, implying near eutectic Sn-Bi composition. In Fig. 8b and d the intensity of Bi(0 1 2) is higher than that of Sn(2 0 0) orientation.

4 Conclusions

Versatile Sn-Bi co-deposition has been demonstrated from a cyanide-free, sulfonic-acid-free, acidic bath using insoluble anodes. Near-eutectic (41.3 %-58.7 % Sn-Bi) and a wide range of (14 to 75 % Sn) compositions have been obtained. Novel morphologies such as yarns of spools have been observed while additives sufficiently homogenize the deposit morphology. Bismuth deposition is a single step, three-electron-transfer and tin deposition is a two-step, four-electron-transfer reduction. While bismuth deposition is diffusion controlled, tin-deposition is kinetically slow. Nitric acid enables co-deposition of bismuth (III) and tin (II) ions from the bath, which is

maintained even with the introduction of bath additives. Increasing the pH selectively inhibits tin deposition. Chronoamperograms corresponding to co-deposition show a sigmoidal variation with time, indicating a complex interplay of the slow tin reduction kinetics, progressive nucleation of the alloys, and the diffusion of ions to the electrode surface. This system shows promise for developing Sn-Bi alloys for microelectronic packaging.

Acknowledgements

The authors thank Amrita Vishwa Vidyapeetham University, the Defence Research Development Organization (DRDO), New Delhi, India, and the Ministry of Human Resources Development (FAST Scheme; F. No. 5-6/2013-TS.VII) for financial support.

References:

- [1] M. Datta, T. Osaka, J. W. Schultze, *New trends in electrochemical technology, Volume 3, Microelectronic packaging*. CRC Press, New York, (2005).
- [2] M. Datta, R. Shenoy, C. Jahnes, P. Andricacos, J. Horkans, J. Dukovic, L. Romankiw, J. Roeder, H. Deligianni, H. Nye, *J. Electrochem. Soc.* **142**, 3779 (1995).
- [3] X. Chen, F. Xue, J. Zhou, S. Liu, G. Qian, *J. Electron. Mater.* **42**, 2708 (2003).
- [4] H-T. Lee, S-Y. Hu, T-F. Hong, Y-F. Chen, *J. Electron. Mater.* **37**, 867 (2008).
- [5] S. Joseph, G. Phatak, K. Gurunathan, T. Seth, D. P. Amalnerkar, T. R. N. Kutty, *J. Appl. Electrochem.* **36**, 907 (2006).
- [6] M. Bigas, E. Cabruja, *Microelectron. J.* **37**, 308 (2006).
- [7] L. Shen, P. Lu, S. Wang, Z. Chen, *J. Alloys Compd.* **574**, 98 (2013).
- [8] M. Abtew, G. Selvaduray, *Mater. Sci. Eng. R-Rep.* **27**, 95 (2000).
- [9] J. Bath, M. Itoh, G. Clark, H. Takahashi, K. Yokota, K. Asai, A. Irisawa, M. Mori, D. Rund, R. Garcia, *As Originally Published in the IPC APEX EXPO Proceedings* (2013).
- [10] M.S. Chandrasekar, M. Pushpavanam, *Electrochim. Acta* **53**, 3313 (2008).
- [11] Y.D. Tsai, C.C. Hu, C.C. Lin, *Electrochim. Acta* **53**, 2040 (2007).
- [12] B. Neveu, F. Lallemand, G. Poupon, Z. Mekhalif, *Appl. Surf. Sci.* **252**, 3561 (2006).
- [13] Y.D. Tsai, C.Y. Yu, C.C. Hu, J.G. Duh, *J. Electrochem. Soc.* **159**, D108 (2011).
- [14] P.E. Bradley, D. Landolt, *Electrochim. Acta* **42**, 993 (1997).
- [15] A. Sharma, S. Bhattacharya, S. Das, K. Das, *Appl. Surf. Sci.* **290**, 373 (2014).
- [16] M. Fukuda, K. Imayoshi, Y. Matsumoto, *Electrochim. Acta* **47**, 459 (2001).
- [17] G. Medvedev, N. Makrushin, A. Dubenkov, *Prot. Met.* **39**, 381 (2003).
- [18] Y.D. Tsai, C.C. Hu, *J. Electrochem. Soc.* **156**, D490 (2009).
- [19] Y.D. Tsai, C.C. Hu, *J. Electrochem. Soc.* **156**, D58 (2009).

- [20] Y-D. Tsai, C-C. Hu, *J. Electrochem. Soc.* **158**, D482 (2011).
- [21] Y. Goh, A. S. M. A. Haseeb, M. F. M. Sabri, *Electrochim. Acta* **90**, 265 (2013).
- [22] Y. Goh, A. S. M. A. Haseeb, H. L. Liew, M. F. M. Sabri, *J. Mater. Sci.* **50**, 4258 (2015).
- [23] M. S. Suh, C. J. Park, H. S. Kwon, *Mater. Chem. Phys.* **110**, 95 (2008).
- [24] M. S. Suh, C. J. Park, H. S. Kwon, *Surf. Coat. Technol.* **200**, 3527 (2006).
- [25] E. Sandnes, M.E. Williams, M.D. Vaudin, G.R. Stafford, *J. Electron. Mater.* **37**, 490 (2008).
- [26] S. Joseph, G. Phatak, *J. Appl. Electrochem.* **42**, 47 (2012).
- [27] S. Joseph, G.J. Phatak, *Surf. Coat. Technol.* **202**, 3023 (2008).
- [28] S. Joseph, G. Phatak, K. Gurunathan, T. Seth, D. P. Amalnerkar, T. R. N. Kutty, *J. Appl. Electrochem.* **36**, 907 (2006).
- [29] E. Sandnes, M. E. Williams, U. Bertocci, M. D. Vaudin, G. R. Stafford, *Electrochim. Acta* **52**, 6221 (2007).
- [30] A. R. Rajamani, U. B. R. Ragula, N. Kothurkar, M. Rangarajan, *CrystEngComm* **16**, 2032 (2014).
- [31] A. R. Rajamani, S. Jothi, M. DhineshKumar, S. Srikaanth, M. K. Singh, G. Otero-Irurueta, D. Ramasamy, M. Datta, M. Rangarajan, *J. Phys. Chem. C* **120**, 22398 (2016).
- [32] R. Buckle, The recovery of metals from waste solutions by electrochemical methods, *Dissertation*, University of Newcastle (2007).
- [33] C.B. Laura, V.F.B. María, A.G. Claudio, E.A. Patricia, A.B. Silvia, *J. Mol. Struct.* **1008**, 95 (2012).
- [34] A. He, Q. Liu, D. Ivey, *J. Mater. Sci. - Mater. Electron.* **19**, 553 (2008).
- [35] E. Asato, K. Katsura, M. Mikuriya, U. Turpeinen, I. Mutikainen, J. Reedijk, *Inorg. Chem.* **34**, 447 (1995).
- [36] A. H. Gregory, M. B. Glen, *Proceedings of the Sixth International Symposium on Electrode Processes*, Wieckowski, A. and Itaya, K., Editors. **96-8**, p. 215, The Electrochemical Society: Los Angeles, CA, (1996).
- [37] M. Summyia, P. Rashida, A. Maria, *Int. J. Chem.* **4**, 15 (2012).
- [38] A. R. Rajamani, Electrodeposition as a synthesis strategy for controlled morphologies and alloy compositions, *Dissertation*, Amrita Vishwa Vidyapeetham, India (2017).
- [39] M. Schlesinger, M. Paunovic, *Modern electroplating*. 5th Edition, Wiley (2010).
- [40] J. Zhang, M. An, L. Chang, *Electrochim. Acta* **54**, 2883 (2009).
- [41] C. Han, Q. Lu, D. G. Ivey, *Electrochim. Acta* **54**, 3419 (2009).
- [42] A. Afshar, A. G. Dolati, M. Ghorbani, *Mater. Chem. Phys.* **77**, 352 (2002).
- [43] M. Palomar-Pardavé, B. R. Scharifker, E. M. Arce, M. Romero-Romo, *Electrochim. Acta* **50**, 4736 (2005).

Figures

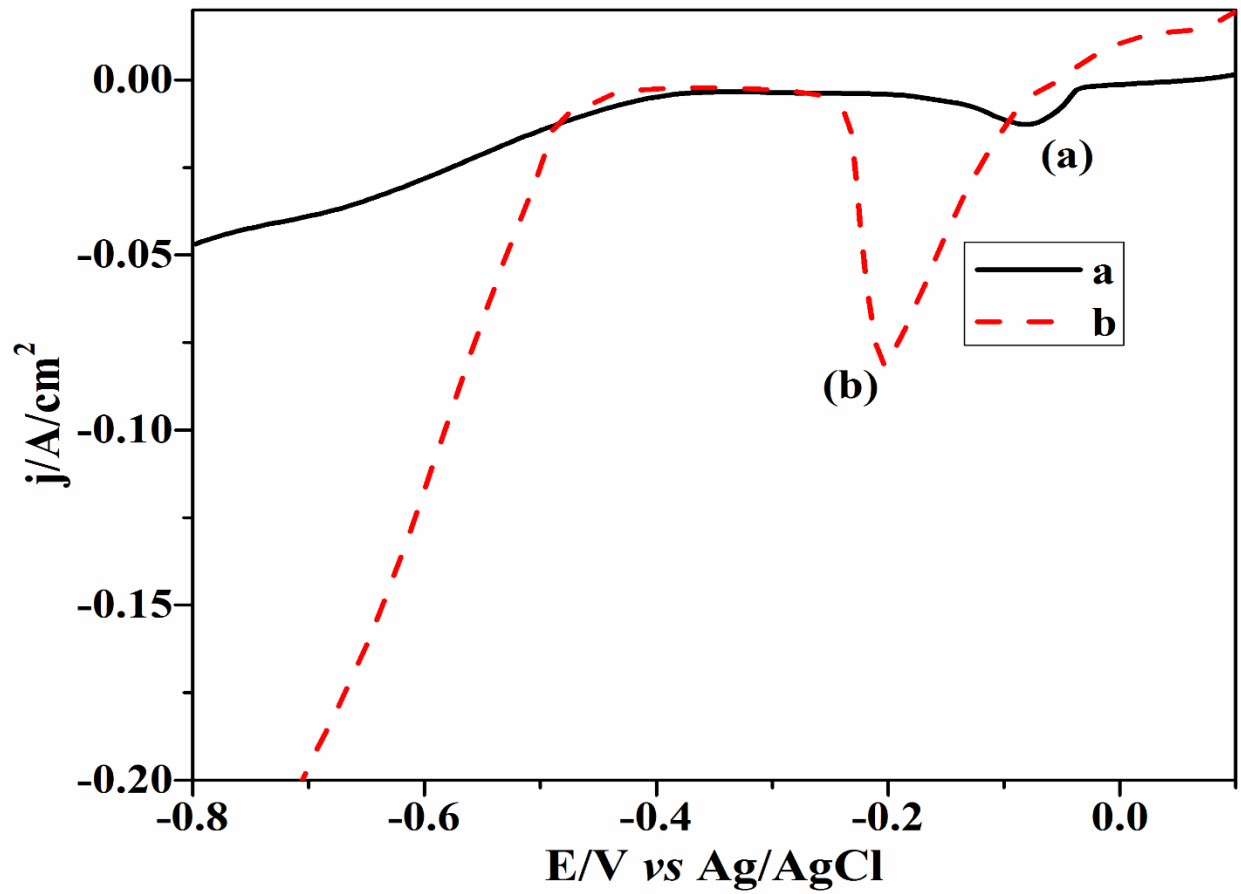


Figure 1. Linear sweep voltammograms of reduction of (a) Bi^{3+} and (b) Sn^{4+} ions on polycrystalline copper at a scan rate of 50 mV/s from a bath containing (a) 0.02 M $\text{Bi}(\text{NO}_3)_3$; (b) 0.2 M SnCl_4

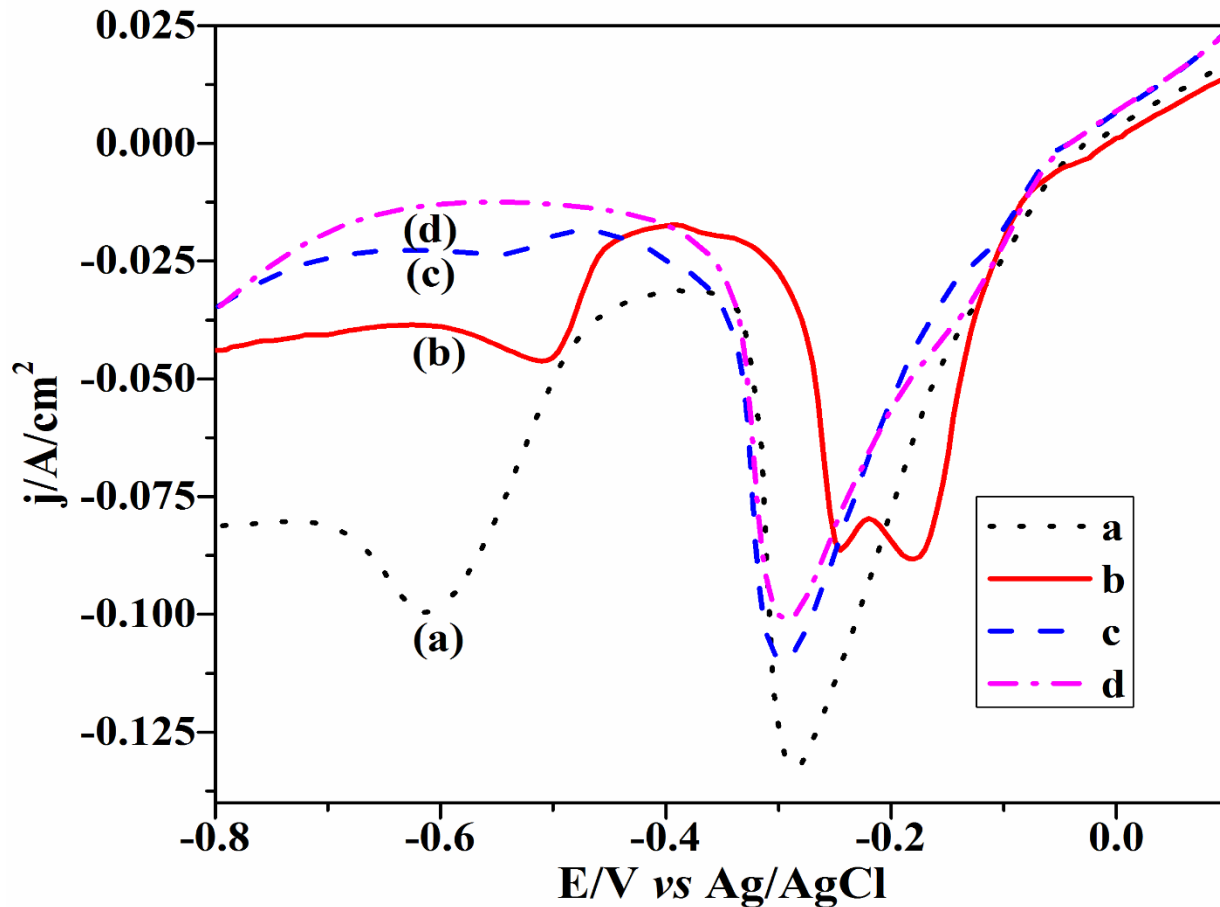


Figure 2. Linear sweep voltammograms of co-reduction of Sn^{4+} and Bi^{3+} ions on polycrystalline copper at a scan rate of 50 mV/s (a) bath containing (a) 0.02 M $\text{Bi}(\text{NO}_3)_3$, 0.2 M SnCl_4 ; (b) 0.02 M $\text{Bi}(\text{NO}_3)_3$, 0.2 M SnCl_4 , 0.2 M citric acid, 5 gpl poly(vinyl alcohol) and 0.05 M betaine, (c) 0.02 M $\text{Bi}(\text{NO}_3)_3$, 0.2 M SnCl_4 , 0.2 M citric acid, 5 gpl poly(vinyl alcohol) and 0.05 M betaine at pH 3.0 (d) 0.02 M $\text{Bi}(\text{NO}_3)_3$, 0.2 M SnCl_4 , 0.2 M citric acid, 5 gpl poly(vinyl alcohol) and 0.05 M betaine at pH 6.0

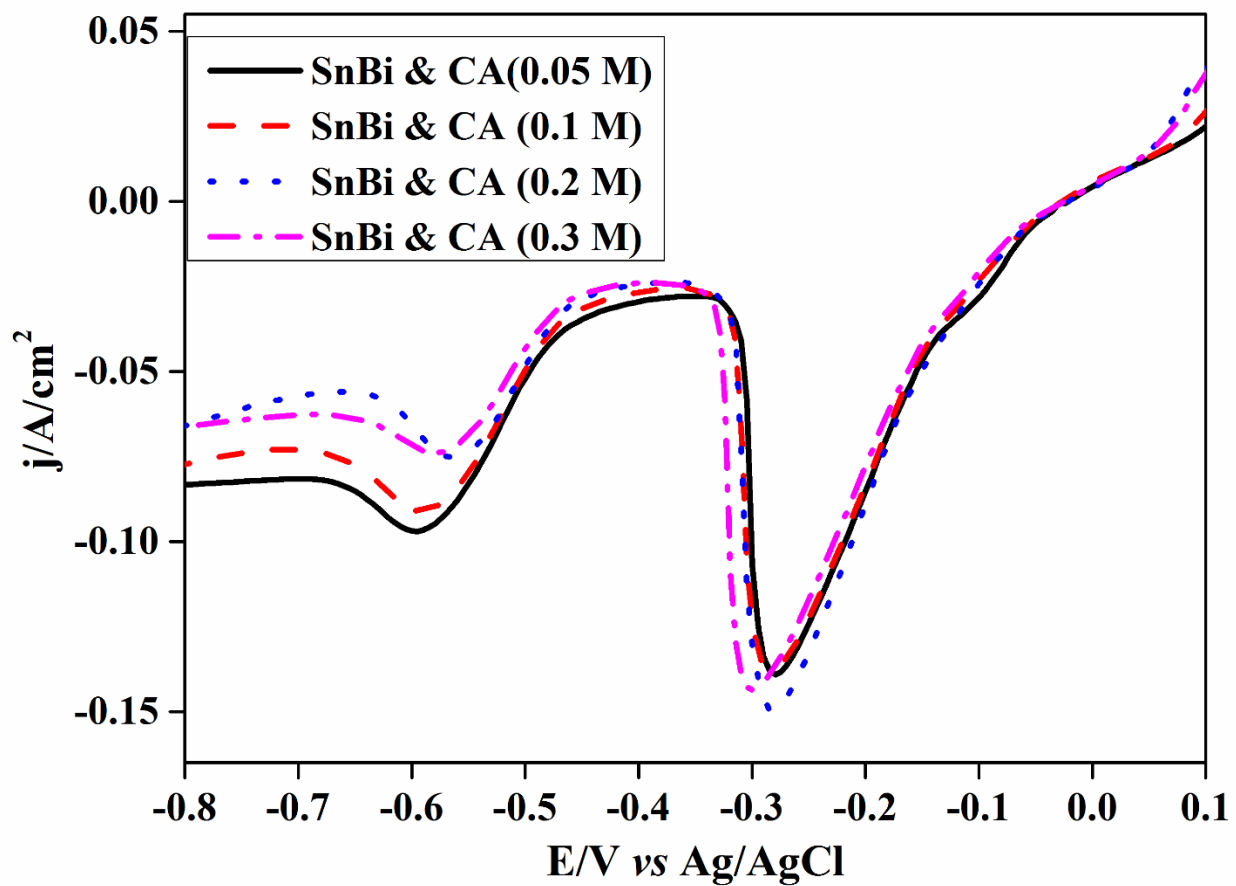


Figure 3. Linear sweep voltammograms of co-reduction of Sn^{4+} and Bi^{3+} ions on polycrystalline copper from a bath containing 0.02 M $\text{Bi}(\text{NO}_3)_3$, 0.2 M SnCl_4 with various concentrations of citric acid (CA) 0.05 M, 0.1 M, 0.2 M, 0.3 M, 0.4 M at a scan rate of 50 mV/s.

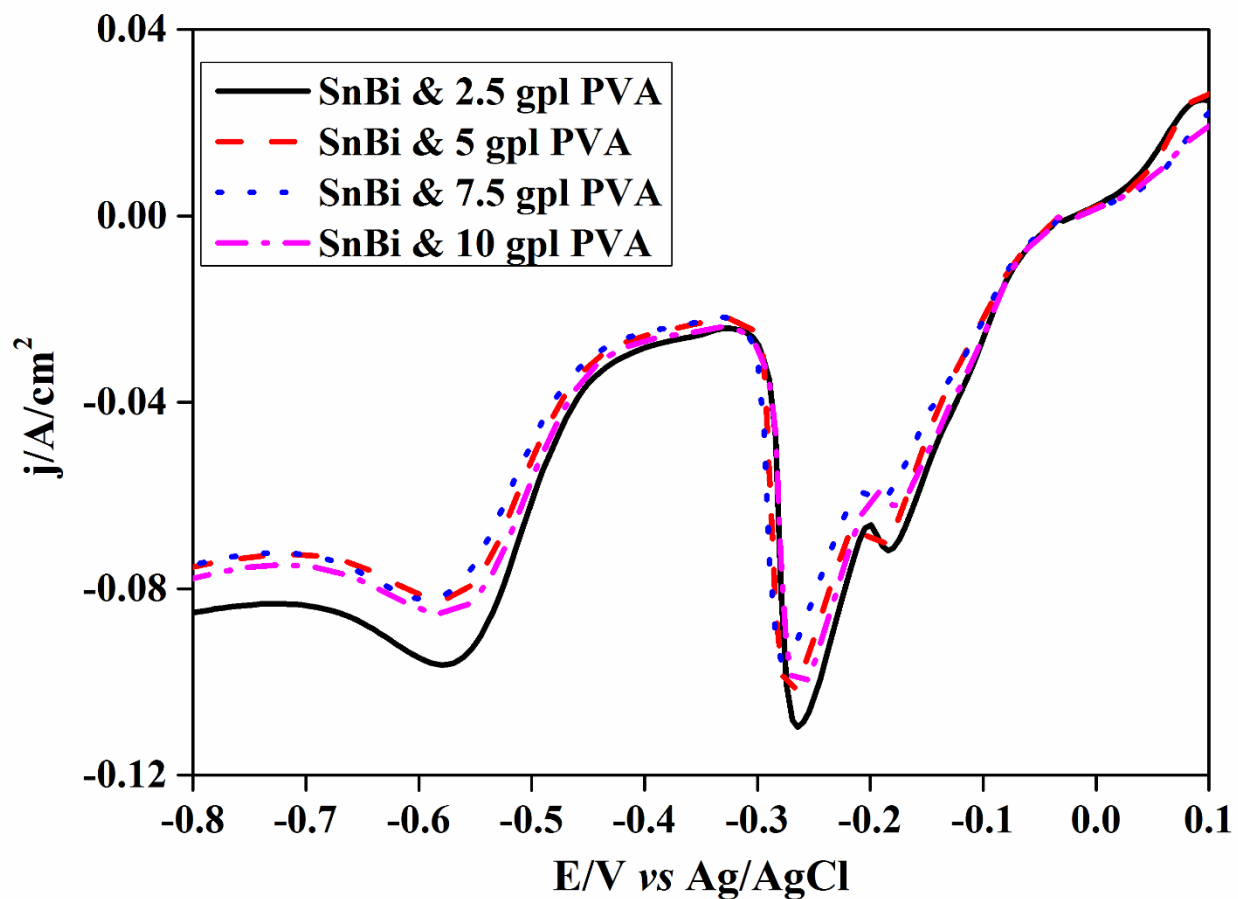


Figure 4. Linear sweep voltammograms of co-reduction of Sn^{4+} and Bi^{3+} ions on polycrystalline copper from a bath containing 0.02 M $\text{Bi}(\text{NO}_3)_3$, 0.2 M SnCl_4 with various concentrations of PVA 2.5, 5, 7.5, 10 gpl at a scan rate of 50 mV/s.

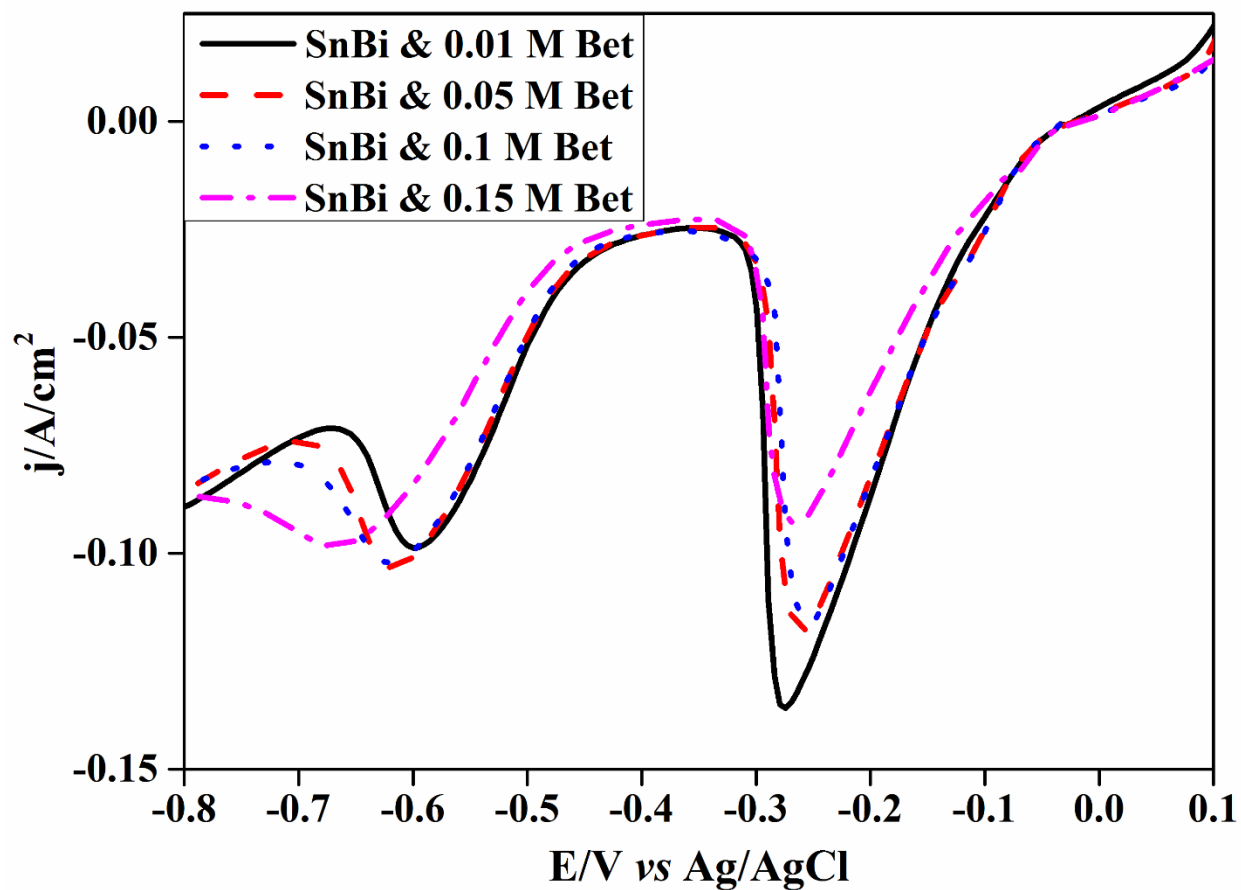


Figure 5. Linear sweep voltammograms of co-reduction of Sn^{4+} and Bi^{3+} ions on polycrystalline copper from a bath containing 0.02 M $\text{Bi}(\text{NO}_3)_3$, 0.2 M SnCl_4 with various concentrations of betaine 0.01 M, 0.05 M, 0.1 M, 0.15 M at a scan rate of 50 mV/s.

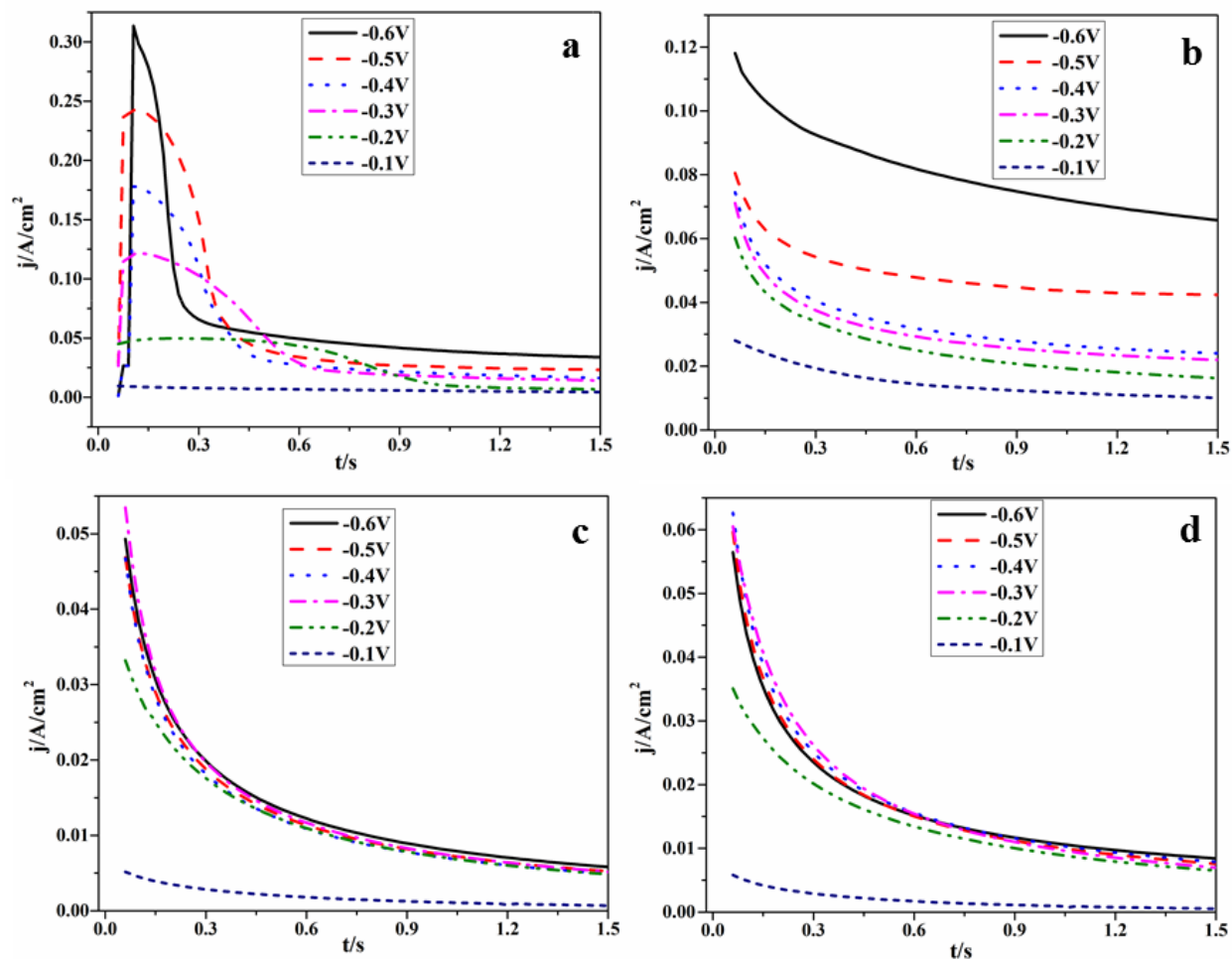
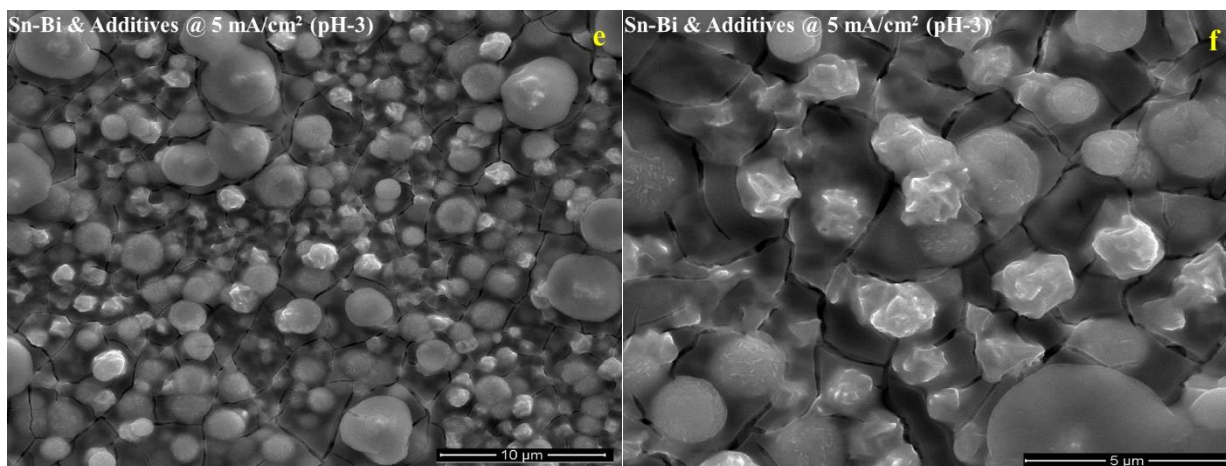
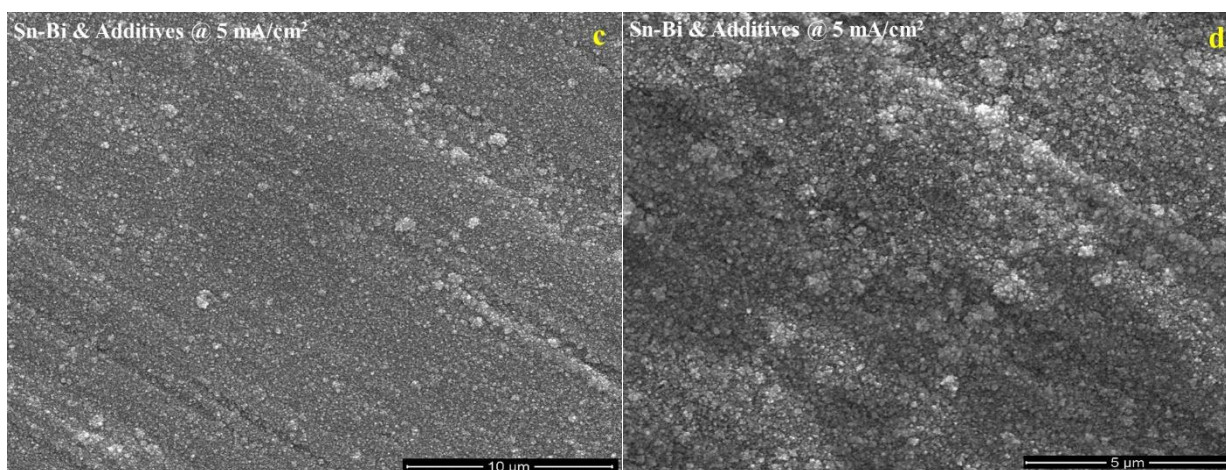
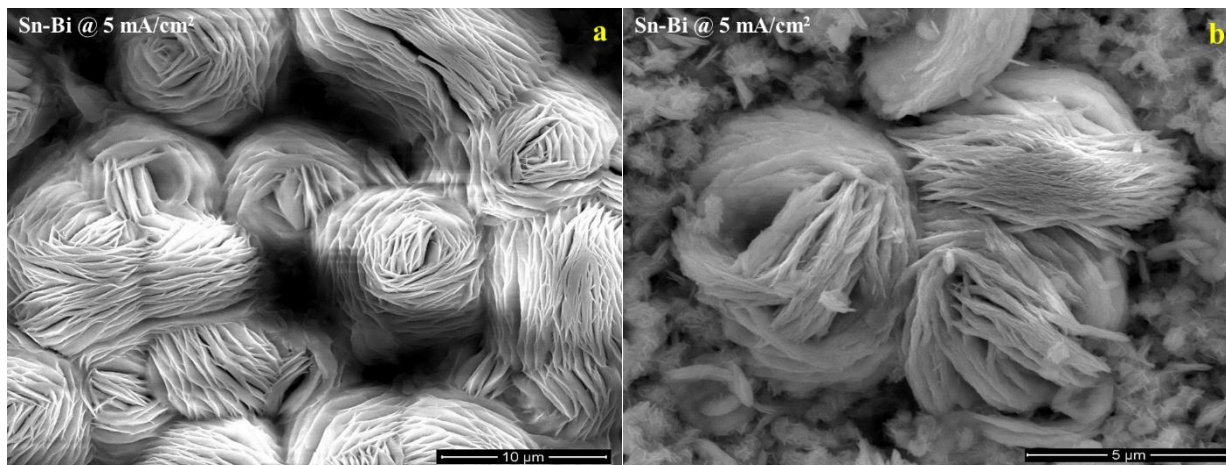


Figure 6. Chronoamperograms of co-reduction of Sn^{4+} and Bi^{3+} ions on polycrystalline copper (a) 0.02 M $\text{Bi}(\text{NO}_3)_3$, 0.2 M SnCl_4 (b) 0.02 M $\text{Bi}(\text{NO}_3)_3$, 0.2 M SnCl_4 , 0.2 M citric acid, 5gpl PVA, and 0.05 M betaine (c) 0.02 M $\text{Bi}(\text{NO}_3)_3$, 0.2 M SnCl_4 , 0.2 M citric acid, 5 gpl PVA, and 0.05 M betaine at pH 3.0 (d) 0.02 M $\text{Bi}(\text{NO}_3)_3$, 0.2 M SnCl_4 , 0.2 M citric acid, 5 gpl PVA, and 0.05 M betaine at pH 6.0 at different potential steps.



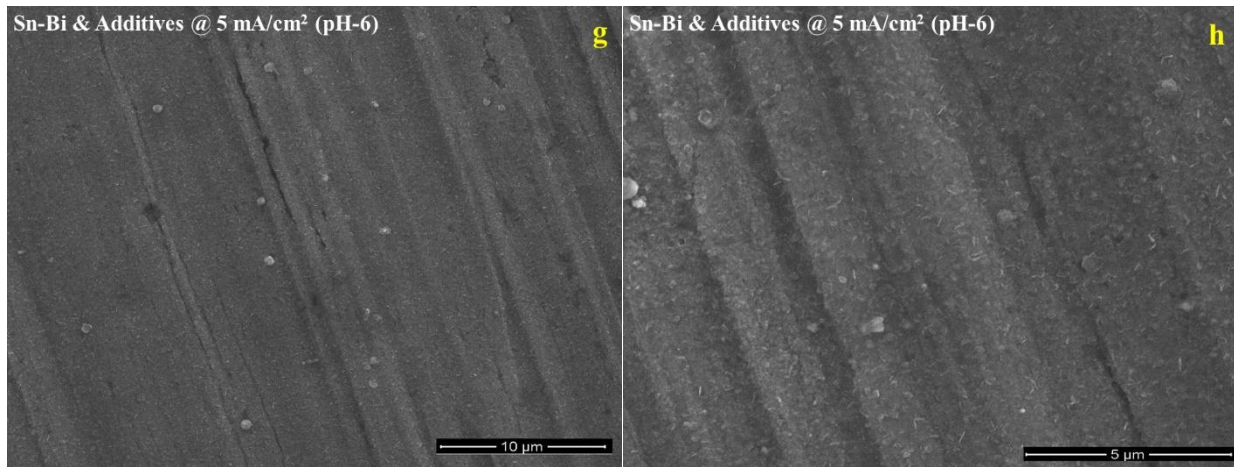


Figure 7. HR-SEM images showing the influence of additives and pH on the morphology of Sn-Bi alloys electrodeposited at 5 mA/cm²; (a&b) Yarn-of-spool morphologies and crystallites (c&d) Sn-Bi alloy and additives (e&f) Sn-Bi alloy and additives at pH 3.0 (g&h) Sn-Bi alloy and additives at pH 6.0

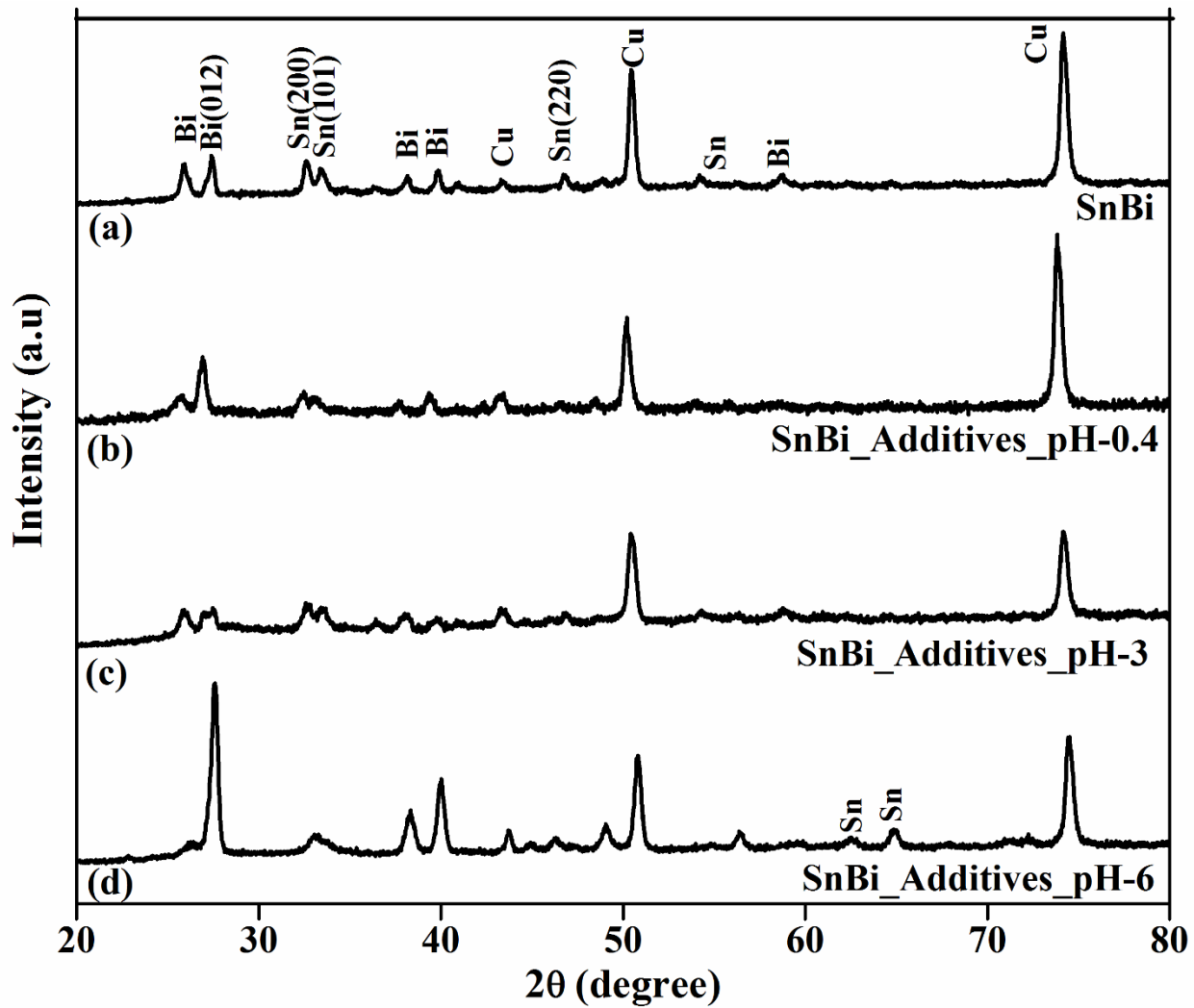


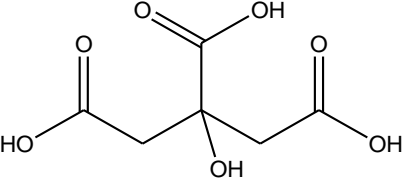
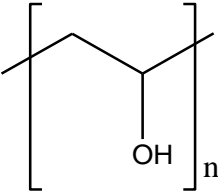
Figure 8(a-d). XRD patterns of Sn-Bi alloy electrodeposits from the bath corresponding to Table 3

Tables

Table 1. Thermomechanical properties of some selected metals, Pb-based, and Pb-free solders applicable in flip-chip interconnection (compiled from multiple sources) [8]

Solder Type	Metal/Alloy	Melting Point (°C)	Young's Modulus (GPa)	Thermal Conductivity (W/mK)
Metal	Lead	328	16	35
	Tin	232	50	66
	Silver	960.8	-	418
	Copper	1083	117	393
	Bismuth	271	32	8.1
	Indium	156.4	11	82.0
Pb based alloy	Sn97Pb	310	22	35
	63Sn37Pb (Eutectic)	183	35	51
Pb-free	Sn3.5Ag (Eutectic)	221	51	56
	Sn3.9Ag0.6Cu	217	51	-
	Sn-Ag-Cu-Zn	217-220	-	-
	Sn-Ag-Cu-Mn	211-215	-	-
	42Sn58Bi (Eutectic)	138	28.5	20
	48Sn52In (Eutectic)	118	23.6	-

Table 2: Typical bath compositions for Sn-Bi alloy electrodeposition

Chemicals/Parameters	Concentration/Conditions	Structures
SnCl ₄ · 5H ₂ O	0.2 M	-
Bi(NO ₃) ₃ · 5H ₂ O	0.02 M	-
Citric acid	0.2 M	
Poly (Vinyl alcohol) PVA	5 gram per liter (gpl)	

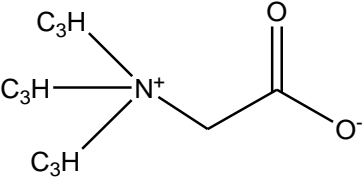
Betaine	0.05 M	
Current density	5 mA/cm ²	-
pH	0.4/3/6	-

Table 3: Reduction potentials of Sn-Bi alloys at different bath conditions

Reduction System	Bi ³⁺ reduction potential (ΔE/mV)	Sn ²⁺ reduction potential (ΔE/mV)	Sn ⁴⁺ reduction potential (ΔE/mV)	Bi ³⁺ reduction current (mA)	Sn ²⁺ reduction current (mA)	Sn ⁴⁺ reduction current (mA)
Bismuth	82	-	-	12.73	-	-
Tin	-	202	502	-	81.36	27.98
Sn-Bi	282		612	132.65		99.52
Sn-Bi Additives	178	243	508	88.26	86.39	46.21
Sn-Bi Additives @ pH 3.0	293		548	109.74		23.53
Sn-Bi Additives @ pH 6.0	293		708	100.94		20.07

Table 4: Compositions of electrodeposited Sn-Bi alloys

Bath conditions	Sn (%)	Bi (%)	Comment
Galvanostatic 5 mA/cm ²			
Sn-Bi Alloy (no additives)	41.3	58.7	Eutectic
Sn-Bi Alloy with additives (pH 0.4)	54.4	45.6	↑ Bi in Deposit
Sn-Bi Alloy with additives (pH 3.0)	36.5	63.5	
Sn-Bi Alloy with additives with pH 6.0	14.0	86.0	
Sn-Bi Alloy with additives (pH 0.4) <i>Potentiostatic: - 0.5 V</i>	74.9	25.1	Sn-rich

ToC Graphic:

